arXiv:2204.00939v1 [cond-mat.mes-hall] 2 Apr 2022

Probing biexciton in monolayer WS_2 through controlled many-body interaction

Suman Chatterjee[1], Sarthak Das[1], Garima Gupta[1],
Kenji Watanabe[2], Takashi Taniguchi[3] and Kausik Majumdar[1*]
[1]Department of Electrical Communication Engineering,
Indian Institute of Science, Bangalore 560012, India
[2]Research Center for Functional Materials,
National Institute for Materials Science, 1-1 Namiki, Tsukuba 305-044, Japan
[3]International Center for Materials Nanoarchitectonics,
National Institute for Materials Science, 1-1 Namiki, Tsukuba 305-044, Japan
*Corresponding author, email: kausikm@iisc.ac.in

April 5, 2022

Abstract

The monolayers of semiconducting transition metal dichalcogenides host strongly bound excitonic complexes and are an excellent platform for exploring many-body physics. Here we demonstrate a controlled kinetic manipulation of the five-particle excitonic complex, the charged biexciton, through a systematic dependence of the biexciton peak on excitation power, gate voltage, and temperature using steady-state and time-resolved photoluminescence (PL). With the help of a combination of the experimental data and a rate equation model, we argue that the binding energy of the charged biexciton is less than the spectral separation of its peak from the neutral exciton. We also note that while the momentum-direct radiative recombination of the neutral exciton is restricted within the light cone, such restriction is relaxed for a charged biexciton recombination due to the presence of near-parallel excited and final states in the momentum space.

Introduction:

Due to strong confinement and relatively large carrier effective mass, monolayers of semiconducting transition metal dichalcogenides (TMDCs) exhibit light-matter interaction strongly driven by excitonic complexes, and are thus an excellent platform for exploring many-body physics at the two-dimension [1–4]. Experimental Observations of neutral bright and dark excitons (X^0 and X_D^0) [1, 4–8], and other excitonic complexes such as positive or negatively changed trion ($X^{\pm}$) [9–13], dark trion ($X_D^{\pm}$) [14–16], neutral biexciton (XX^0) [6] and charged biexciton($XX^{\pm}$) [6, 17, 18] have been widely reported. One recent report also explained electroluminescence from exciton and its complexes [19]. The charged biexciton is of particular interest, which is a five-particle complex, consisting of two holes and three electrons (XX^-) or three holes and two electrons (XX^+) bound through coulomb interaction, and are distinct from the neutral biexciton. Due to the specific formation and recombination kinetics, the rate equations dictate a square law dependence between the exciton and biexciton intensities [20–24]. This makes the biexciton the strongest emitting complex among all the observable excitonic complexes at higher excitation density [18, 22, 25, 26]. Besides, the charged nature of the $XX^{\pm}$ species makes it amenable to be controlled by a gate voltage [6, 18].

The identification of biexciton by superlinear power-law [6, 17, 18, 21, 22], its coherent formation from two excitons [27], and the binding energy [28, 29] have been discussed in the recent literature. For tungsten-based TMDC, the neutral versus charged biexciton can be distinguished [6, 30]. Interestingly, several of these works report a power law with exponent in the range of 1.4-1.6 for the charged biexciton [6, 22, 25, 30], which is significantly less than 2 - a physical explanation of the same will be desirable. Besides, a detailed understanding of the formation and recombination kinetics will be widely useful in the context of the biexciton. We address these questions in the present work.

Results and Discussions:

We probe the biexciton states using steady-state and time-resolved photoluminescence (PL) measurement. The lowest excitonic state in 1L-WS_2 is spin-dark due to its unique spin-split bands at $K(K')$ valleys [5, 7, 31, 32]. Under the steady-state condition, as a result of a larger

radiative lifetime of the dark exciton state [15, 32, 33], a large fraction of the light-emitting neutral biexcitons (XX^0) form through each pair of spin-bright and spin-dark excitonic states, as opposed to both being bright exciton [6,14]. Further, in the presence of doping, the formation of a five-particle charged biexciton ($XX^{\pm}$) is favored. There likely exists a larger steady-state density of completely dark charged-biexciton (forming from a dark exciton and a dark trion) in WS_2, though it does not contribute to the PL signal.

To identify the type of biexcitons (XX^0 or $XX^{\pm}$) in our experiment, we prepare an Au/hBN/1L-WS_2/hBN (sample D1, represented in Figure 1a-b) using dry transfer method (see **Methods** for sample preparation). A gate voltage (V_g) is applied to the bottom Au electrode, while connecting the WS_2 layer to a grounded few-layer graphene contact. The V_g dependent PL spectra, taken at 4 K, is shown in a color plot in Figure 1c (see **Supporting Information Figure 1** for representative spectra and fitted peak intensity values), suggesting a strong modulation of the neutral exciton (X^0), trion (X^-) and XX^- peak intensity, in good agreement with previous reports [18,23,25,34]. With $V_g > 0$, the intensity of X^0 is suppressed, while that of X^- is enhanced. The XX^- peak is observed in the V_g range where both X^0 and X^- have PL signatures, suggesting the origin of the five-particle state from the neutral and charged excitons. Note that the maximum intensity of the XX^- occurs at a slightly higher positive V_g compared to the maximum intensity of X^0. Such a reduction in the X^0 intensity at the maximum XX^- intensity point results from a non-radiative loss of the excitons towards formation of trions and charged biexcitons.

Figure 2a schematically depicts the formation process of the charged biexciton where a dark trion (X_D^-) [15, 35] and a bright X^0 collide over a cross-section at the band edge, and form a XX^- with kinetic energy ΔE_{XX^-}, along with emitting a phonon of energy $\hbar\omega_f$. This leads to

$$E_{X^0} + E_{X_D^-} = E_{XX^-}(\mathbf{Q}=\mathbf{0}) + \underbrace{\Delta E_{XX^-}(\mathbf{Q}) + \hbar\omega_f}_{E_b} \tag{1}$$

Here, E_{X^0}, $E_{X_D^-}$ and E_{XX^-} are the energies of the bright exciton, dark trion and charged biexciton, respectively. By this process the dark trion and the bright exciton bind together

with a binding energy given by

$$E_b = \Delta E_{XX^-}(\mathbf{Q}) + \hbar\omega_f \tag{2}$$

During recombination at finite $\mathbf{Q}$, there is a direct transition from the XX^- band to the X_D^- band, emitting a photon of energy $\hbar\omega$, leading to

$$E_{XX^-}(\mathbf{Q}=\mathbf{0}) + \Delta E_{XX^-}(\mathbf{Q}) = E_{X_D^-}(\mathbf{Q}=\mathbf{0}) + \Delta E_{X_D^-}(\mathbf{Q}) + \hbar\omega \tag{3}$$

where $\Delta E_{X_D^-}(\mathbf{Q})$ is the recoil energy of the remaining dark trion. There is a striking difference in the final states of the biexciton and the exciton recombination process. Linear momentum conservation forces all recombination giving out a photon to occur within the light cone of the exciton band around $\mathbf{Q} = \mathbf{0}$ [36, 37]. However, such constraint is relaxed for the biexciton recombination. Since the final state (X_D^-) is varying in energy with Q, the recombination process of XX^- can also take place at varying Q, as long as the final state is empty and the transition is allowed. This can be visualized as multiple light cones, schematically depicted in Figure 2b.

Combining Equations 1, 2, and 3, we get

$$E_b = (E_{X^0} - \hbar\omega) - [\Delta E_{X_D^-}(\mathbf{Q}) - \Delta E_{XX^-}(\mathbf{Q})] \tag{4}$$

Note that XX^- being a heavier particle than X_D^-, the bands are non-parallel with $\Delta E_{X_D^-}(\mathbf{Q}) - \Delta E_{XX^-}(\mathbf{Q}) \approx \frac{\hbar^2 Q^2}{15 m_0} > 0$ for non-zero $\mathbf{Q}$ (assuming $m_e = m_h \approx 0.5 m_0$). Thus the binding energy of the biexciton is less than the separation between the exciton and the biexciton PL emission peaks ($E_{X^0} - \hbar\omega > E_b$), with the deviation being quadratic in Q.

In order to establish this, in Figure 2c, we show the temperature-dependent PL intensity variation of X^0 and XX^-, obtained from PL spectra from a Ag/hBN/1L-WS_2/hBN stack (sample D2, see **Supporting Information Figure 2a and b** for device schematic and optical image) with no active gating and keeping WS_2 electrically floating. The thickness of the bottom and top hBN layer is kept in the range of 25-30 nm and 10-15nm, respectively. The thickness is chosen to enhance the signal through constructive interference in the stack [38, 39]. We

observe the charged biexciton emission up to a sample temperature of 130 K. The Ag layer provides a pathway for fast dissipation of locally generated heat due to the focussed laser spot, thus helping to suppress laser-induced local heating. The separation between the exciton and charged biexciton peaks ($E_{X^0} - \hbar\omega$) is $60 \pm 5\ meV$. The plot of intensity variation of X^0 peak as a function of T in Figure 2c shows an increasing trend with T. We attribute this to the fact that the bright exciton being energetically higher than the dark exciton state in W-based TMDCs [5, 7, 15]. However, the XX^- peak shows the opposite trend, with sharply decreasing peak intensity (see **Supporting Information Figure 3a and b** for model spectrum fitting and temperature-dependent spectra respectively) as temperature increases, in agreement with previous reports [17,30]. The data fits well with an equation of the form [40,41] (see **Supporting Information S1**):

$$\eta(T) = \frac{1}{1 + \kappa e^{-E_b/k_B T}} \tag{5}$$

suggesting an enhanced thermal dissociation of XX^- at higher temperature. From the fit, we estimate a value of E_b in the range of 40 ± 5 meV, which is less (15 - 20 meV) than the peak separation in the PL spectra, and in agreement with our previous assertion $E_{X^0} - \hbar\omega > E_b$.

To understand the strong temperature dependence of the kinetics of the charged biexciton population, we write the rate equations using the formation of this five particle complex from its constituent particles [6, 20]:

$$dn_{X^0}/dt = -n_{X^0}/\tau_{X^0} + \beta_1 P + \gamma_2 n_f n_{XX^-} e^{\frac{-\Delta E_{XX^-}}{k_B T}} - \beta_2 n_{X^0} - \gamma_1 (n_f + 1) n_{X^0} n_{X_D^-} \tag{6}$$

$$dn_{X_D^-}/dt = -n_{X_D^-}/\tau_{X_D^-} + \beta_2 n_{X^0} + \gamma_2 n_f n_{XX^-} e^{\frac{-\Delta E_{XX^-}}{k_B T}} + n_{XX^-}/\tau_{XX^-} - \gamma_1 (n_f + 1) n_{X^0} n_{X_D^-} \tag{7}$$

$$dn_{XX^-}/dt = -n_{XX^-}/\tau_{XX^-} + \gamma_1 (n_f + 1) n_{X^0} n_{X_D^-} - \gamma_2 n_f n_{XX^-} e^{\frac{-\Delta E_{XX^-}}{k_B T}} \tag{8}$$

The parameters β_1,β_2, γ_1 and γ_2 are proportional to the quantum efficiency of creation of X^0 from incident photons, the rate of decay of X^0 to X_D^- population, the rate of XX^- creation and the rate of XX^- dissociation, respectively. n_f is the phonon number. n_{X^0}, $n_{X_D^-}$ and n_{XX^-} represent density of the respective excitonic species. τ_{X^0}, $\tau_{X_D^-}$ and τ_{XX^-} represent radiative lifetime of bright exciton, dark trion and biexciton respectively.

The steady-state solution of the set of equations, if thermal-equilibrium phonon distribution

(Bose-Einstein distribution) is considered, predicts $n_{XX^-} \propto n_{X^0}^2$, that is, a square-law dependence of biexciton population with respect to exciton population. However, with higher incident photon flux, every biexciton formation gives rise to the emission of a phonon. Since phonons are relatively long-lived, n_f deviates from equilibrium Bose-Einstein distribution. Under such a condition, we approximate $n_f \propto n_{XX^-}$. This leads to a generation of the non-equilibrium hot phonon density, which in turn triggers an efficient dissociation of XX^-, forcing a deviation from quadratic law. In this condition, we obtain (see **Supporting Information S2** for detailed calculation):

$$An_{XX^-} + Bn_{XX^-}^2 exp(-\Delta E_{XX^-}/k_BT) = n_{X^0}^2 \tag{9}$$

with $A = \frac{1}{\tau_{XX^-}\gamma_1(n_f+1)\beta_2\tau_{X_D^-}}$ and $B = \frac{\gamma_2\tau_{XX^-}}{\tau_{XX^-}\gamma_1(n_f+1)\beta_2\tau_{X_D^-}}$
This establishes a one-to-one correspondence between charged biexciton (n_{XX^-}) and bright exciton (n_{X^0}) population and clearly indicates a deviation from the near-equilibrium square law dependence at for $T > 0$. Equation 9 also suggests that the corresponding kinetics can be tuned by external stimulus. Note that the primary temperature dependence arises from the factor $e^{\frac{-\Delta E_{XX^-}}{k_BT}}$, while other parameters are very weak function of temperature. Accordingly, with an increase in temperature, the second term on the left-hand side starts dominating, and the equation becomes linear.

To verify this temperature dependent coupled exciton - charged biexciton kinetics, we probe the excitation power (P) dependence of the PL spectra (on sample D2) from $T = 4.2$ to 70 K (representative spectra shown in **Supporting Information Figure 4**). Experimentally obtained X^0 and XX^- PL intensities are fitted with equation 9 using A and B as parameters, shown in Figure 3a. The best fit is obtained at $\Delta E_{XX^-} \approx 10$ meV. It is evident from equation 9 that a power law type relation such as $I_{XX^-} \propto I_{X^0}^{\alpha}$ does not exactly hold. However, the value of α from such a relation provides a quick qualitative understanding, and helps to compare with existing reports in literature. Figure 3b represents such a power law fitting at 4 and 10 K (Fittings at higher temperature values with equation 9 and $I_{XX^-} \propto I_{X^0}^{\alpha}$ are shown in **Supporting Information Figure 5**). The obtained α values are plotted as a function of temperature in Figure 3c (XX^- intensity variation with laser power (P) at different temperature points is

fitted with $I_{XX^-} \propto P^{\alpha}$ and represented in **Supporting Information Figure 6a and b**). We observe that α sharply drops with an increase in temperature, suggesting that the second term in the left-hand side of equation 9 dominates the other term at a higher temperature (This power law measurement is repeated for sample D1, which is the stack used for gating and fitted with $I_{XX^-} \propto I_{X^0}^{\alpha}$ lines. Obtained α values are shown in **Supporting Information Figure 10**).

To further investigate the temperature dependence of the XX^- kinetics, we perform time-resolved photoluminescence (TRPL) measurement of 1L WS_2 at different T. We excite the sample with a 531 nm pulsed laser (Average optical power of 17 μW) with an FWHM of 48 ps and a repetition rate of 5 MHz. The instrument response function (IRF) shows a full-width-at-half-maximum (FWHM) of 52 ps and a decay of 23 ps (See **Methods** for details about measurement technique). To filter out XX^- luminescence only, we use a bandpass filter (10 nm passband) centered at 610 nm. The *in situ* steady-state PL spectra obtained at different temperatures are shown in **Supporting Information Figure 8**, with the filter window marked. The time-dependent emission from the XX^- peak at different temperatures is shown (in symbols) in Figure 4a. To obtain the decay time of XX^-, we fit (solid lines) the measured TRPL data using two exponentials ($\sum_{i=1}^{2} A_i e^{-t/\tau_i}$) after deconvoluting from the IRF as implemented in QuCoa software (PicoQuant). We note that the faster (and stronger) component (τ_1) that represents the charged biexciton decay is strongly dependent on T. In Figure 4b we plot it as a function of T, which indicates that the net lifetime of the XX^- becomes shorter with increasing T. In particular, we estimate $\tau_1 \approx 25 \pm 0.7$ ps at 6.6 K [23, 42] and $\approx 5 \pm 0.13$ ps at 32 K. Such a reduction in the lifetime is in excellent agreement with equation 9 and the results in Figure 3c, clearly suggesting a fast dissociation of XX^- as temperature increases. It is instructive to consider the situation as follows: since both X_D^- and bright X^0 are present in the system in a large number, the formation of XX^- is not hindered. However, once the rapid dissociation starts at a higher temperature, it provides a fast non-radiative channel giving rise to reduced intensity, small lifetime, and near-unity power law. We also note that there exists a weak (with relative weightage of $A_1/A_2 \approx 10 - 100$), slower decay component with $\tau_2 \sim 50 - 100$ ps. We believe this results from the tail of defect-bound excitonic complexes (see **Supporting Information Figure 8**), usually observed in WS_2.

Finally, we show that the XX^- kinetics can further be modulated by a gate voltage as well, as predicted from equation 9. In Figure 5a, for every V_g value, the incident laser power (P) is varied, and the PL intensity of charged biexciton (I_{XX^-}) is fitted with exciton intensity (I_{X_0}) using the approximate relation $I_{XX^-} \propto I_{X_0}^{\alpha}$ lines (fitting with $I_{XX^-} = P^{\alpha}$ lines is shown in **Supporting information Figure 9**). Variation of α exponents as a function of V_g is shown in Figure 5b. We note that the maximum occurs near $V_g = 0$. Such a strong modulation of the XX^- kinetics can be understood by using equation 9. An increase in $|V_g|$, in turn, enhances the screening in the sample. This affects the stability of XX^- which is of large Bohr radius and relatively weak binding energy. This also triggers an easier dissociation of the charged biexciton (XX^-). Hence, the parameter γ_2 increases driving the power-law exponent towards unity.

In conclusion, we showed that strong non-equilibrium explains the deviation of the charged biexciton intensity from a square-law dependence on the exciton intensity. The nature of dependence can be modulated by external stimuli, such as gate voltage and temperature. Unlike the neutral exciton, the existence of near-parallel bands between excited and final states for the biexciton removes the usual "light-cone" restriction during direct radiative recombination. Consequently, the binding energy of the five-particle species is shown to be less than its peak separation from the neutral exciton. The temperature-dependent enhancement of the decay rate of the charged biexciton further supports the rate equation model. The findings elucidate a deeper understanding of biexciton kinetics in monolayer semiconductors.

Methods:

Fabrication: Au/Ag lines are defined by optical lithography using a 360 nm UV source and AZ5214E resist spin-coated on a Si/SiO2 substrate with 285 nm thick oxide formed by dry chlorinated thermal oxidation and forming gas annealing. A 20 nm thick Ni film followed by a 40 nm thick Au/Ag film is deposited via DC magnetron sputtering and lifted off by acetone/isopropyl alcohol rinse to form the bottom contact. For device D1, first, a few-layer hBN is exfoliated from bulk crystals and subsequently transferred to a poly dimethyl-siloxane (PDMS) sheet. Then it is transferred onto lithographically pre-patterned Au electrodes using dry-transfer technique. The thickness of the flake is identified by optical contrast. In the second

step, 1L WS_2 flake was transferred and connected with another Au electrode using few-layer graphene. Then top hBN is transferred onto the stack following the same procedure. The device was annealed after each layer transfer at 80°C for better adhesion. For device D2, a similar layer-by-layer transfer procedure was followed, except Ag pre-patterned electrodes were used instead of Au ones, and a graphene transfer step was not needed.

PL measurement: The devices are loaded or are wire bonded to a closed-cycle optical top window He cryostat and are illuminated with 532 nm continuous wave laser through ×50 objective lens having a numerical aperture of 0.5. Keithley 2636B is used as a DC voltage source for applying gate voltage (V_g) to vary the doping in device D1. The steady-state PL response of devices (D1 and D2) is analyzed using a spectrometer with 1800 lines/mm grating. All the measurements are performed in a vacuum with a pressure $< 10^{-4}$ Torr.

TRPL measurement: We excite the sample with a 531 nm pulsed laser having full-width-at-half-maximum (FWHM) of 48 ps and a repetition rate of 5 MHz. The sync signal from the laser driver is fed to channel 0 of a TCSPC (PicoHarp 300). The emission from the sample is fed to a single photon detector (Micro Photon Devices), the output of which is connected to channel 1 of the TCSPC. The instrument response function (IRF) shows an FWHM of 52 ps and a decay timescale of 23 ps. Using deconvolution, we can accurately estimate down to 10% of the IRF width [43]. To filter out XX^- luminescence only, we use a bandpass filter (FWHM of 10 nm) centered at 610 nm. For *in situ* steady-state PL spectra, a 50:50 beam splitter is used to divert part of the emission to a spectrometer.

ACKNOWLEDGMENTS:

Growth of hexagonal boron nitride crystals was supported by the Elemental Strategy Initiative conducted by the MEXT, Japan, Grant Number JPMXP0112101001, JSPS KAKENHI Grant Number JP20H00354 and JP19H05790. K.M. acknowledges the support from a grant from Science and Engineering Research Board (SERB) under Core Research Grant, a grant from the Indian Space Research Organization (ISRO), a grant from MHRD under STARS, and support from MHRD, MeitY, and DST Nano Mission through NNetRA.

Competing Interests

The authors declare no competing financial or non-financial interests.

Data Availability

Data available on reasonable request from the corresponding author.

References

[1] Alexey Chernikov, Timothy C Berkelbach, Heather M Hill, Albert Rigosi, Yilei Li, Ozgur Burak Aslan, David R Reichman, Mark S Hybertsen, and Tony F Heinz. Exciton binding energy and nonhydrogenic rydberg series in monolayer WS_2. Physical review letters, 113(7):076802, 2014.

[2] Timothy C Berkelbach, Mark S Hybertsen, and David R Reichman. Theory of neutral and charged excitons in monolayer transition metal dichalcogenides. Physical Review B, 88(4):045318, 2013.

[3] Miguel M Ugeda, Aaron J Bradley, Su-Fei Shi, H Felipe, Yi Zhang, Diana Y Qiu, Wei Ruan, Sung-Kwan Mo, Zahid Hussain, Zhi-Xun Shen, et al. Giant bandgap renormalization and excitonic effects in a monolayer transition metal dichalcogenide semiconductor. Nature materials, 13(12):1091–1095, 2014.

[4] Sarthak Das, Garima Gupta, and Kausik Majumdar. Layer degree of freedom for excitons in transition metal dichalcogenides. Physical Review B, 99(16):165411, 2019.

[5] Xiao-Xiao Zhang, Yumeng You, Shu Yang Frank Zhao, and Tony F Heinz. Experimental evidence for dark excitons in monolayer WSe_2. Physical review letters, 115(25):257403, 2015.

[6] Ziliang Ye, Lutz Waldecker, Eric Yue Ma, Daniel Rhodes, Abhinandan Antony, Bumho Kim, Xiao-Xiao Zhang, Minda Deng, Yuxuan Jiang, Zhengguang Lu, et al. Efficient generation of neutral and charged biexcitons in encapsulated WSe_2 monolayers. Nature communications, 9(1):1–6, 2018.

[7] Xiao-Xiao Zhang, Ting Cao, Zhengguang Lu, Yu-Chuan Lin, Fan Zhang, Ying Wang, Zhiqiang Li, James C Hone, Joshua A Robinson, Dmitry Smirnov, et al. Magnetic brightening and control of dark excitons in monolayer WSe_2. Nature nanotechnology, 12(9):883–888, 2017.

[8] Keliang He, Nardeep Kumar, Liang Zhao, Zefang Wang, Kin Fai Mak, Hui Zhao, and Jie Shan. Tightly bound excitons in monolayer WSe_2. Physical review letters, 113(2):026803, 2014.

[9] Kin Fai Mak, Keliang He, Changgu Lee, Gwan Hyoung Lee, James Hone, Tony F Heinz, and Jie Shan. Tightly bound trions in monolayer MoS_2. Nature materials, 12(3):207–211, 2013.

[10] Akshay Singh, Galan Moody, Kha Tran, Marie E Scott, Vincent Overbeck, Gunnar Berghäuser, John Schaibley, Edward J Seifert, Dennis Pleskot, Nathaniel M Gabor, et al. Trion formation dynamics in monolayer transition metal dichalcogenides. Physical Review B, 93(4):041401, 2016.

[11] Sangeeth Kallatt, Sarthak Das, Suman Chatterjee, and Kausik Majumdar. Interlayer charge transport controlled by exciton–trion coherent coupling. npj 2D Materials and Applications, 3(1):1–8, 2019.

[12] Gerd Plechinger, Philipp Nagler, Ashish Arora, Robert Schmidt, Alexey Chernikov, Andrés Granados Del Águila, Peter CM Christianen, Rudolf Bratschitsch, Christian Schüller, and Tobias Korn. Trion fine structure and coupled spin–valley dynamics in monolayer tungsten disulfide. Nature communications, 7(1):1–9, 2016.

[13] Sarthak Das, Sangeeth Kallatt, Nithin Abraham, and Kausik Majumdar. Gate-tunable trion switch for excitonic device applications. Physical Review B, 101(8):081413, 2020.

[14] Zhipeng Li, Tianmeng Wang, Zhengguang Lu, Mandeep Khatoniar, Zhen Lian, Yuze Meng, Mark Blei, Takashi Taniguchi, Kenji Watanabe, Stephen A McGill, et al. Direct observation of gate-tunable dark trions in monolayer WSe_2. Nano letters, 19(10):6886–6893, 2019.

[15] M Zinkiewicz, AO Slobodeniuk, T Kazimierczuk, P Kapuściński, K Oreszczuk, M Grzeszczyk, M Bartos, K Nogajewski, K Watanabe, T Taniguchi, et al. Neutral and charged dark excitons in monolayer WS_2. Nanoscale, 12(35):18153–18159, 2020.

[16] Erfu Liu, Jeremiah van Baren, Zhengguang Lu, Mashael M Altaiary, Takashi Taniguchi, Kenji Watanabe, Dmitry Smirnov, and Chun Hung Lui. Gate tunable dark trions in monolayer WSe_2. Physical review letters, 123(2):027401, 2019.

[17] Yumeng You, Xiao-Xiao Zhang, Timothy C Berkelbach, Mark S Hybertsen, David R Reichman, and Tony F Heinz. Observation of biexcitons in monolayer WSe_2. Nature Physics, 11(6):477–481, 2015.

[18] Matteo Barbone, Alejandro R-P Montblanch, Dhiren M Kara, Carmen Palacios-Berraquero, Alisson R Cadore, Domenico De Fazio, Benjamin Pingault, Elaheh Mostaani, Han Li, Bin Chen, et al. Charge-tuneable biexciton complexes in monolayer WSe_2. Nature communications, 9(1):1–6, 2018.

[19] Matthias Paur, Aday J Molina Mendoza, Rudolf Bratschitsch, Kenji Watanabe, Takashi Taniguchi, and Thomas Mueller. Electroluminescence from multi-particle exciton complexes in transition metal dichalcogenide semiconductors. Nature communications, 10(1):1–7, 2019.

[20] VM Asnin, BV Zusov, TM Murina, AM Prokhorov, AA RooAcHEv, and NI Sablina. Radiative recombination of biexcitons in germanium. SOVIET PHYSICS JETP, 35(2), 1972.

[21] JR Haynes. Experimental proof of the existence of a new electronic complex in silicon. Physical Review Letters, 4(7):361, 1960.

[22] Jiajie Pei, Jiong Yang, Xibin Wang, Fan Wang, Sudha Mokkapati, Tieyu LuHERE!HERE!, Jin-Cheng Zheng, Qinghua Qin, Dragomir Neshev, Hark Hoe Tan, et al. Excited state biexcitons in atomically thin $MoSe_2$. ACS nano, 11(7):7468–7475, 2017.

[23] Philipp Nagler, Mariana V Ballottin, Anatolie A Mitioglu, Mikhail V Durnev, Takashi Taniguchi, Kenji Watanabe, Alexey Chernikov, Christian Schüller, Mikhail M Glazov,

Peter CM Christianen, et al. Zeeman splitting and inverted polarization of biexciton emission in monolayer WS_2. Physical review letters, 121(5):057402, 2018.

[24] RT Phillips, DJ Lovering, GJ Denton, and GW Smith. Biexciton creation and recombination in a gaas quantum well. Physical Review B, 45(8):4308, 1992.

[25] Gerd Plechinger, Philipp Nagler, Julia Kraus, Nicola Paradiso, Christoph Strunk, Christian Schüller, and Tobias Korn. Identification of excitons, trions and biexcitons in single-layer WS_2. physica status solidi (RRL)–Rapid Research Letters, 9(8):457–461, 2015.

[26] Edbert J Sie, Alex J Frenzel, Yi-Hsien Lee, Jing Kong, and Nuh Gedik. Intervalley biexcitons and many-body effects in monolayer MoS_2. Physical Review B, 92(12):125417, 2015.

[27] Alexander Steinhoff, Matthias Florian, Akshay Singh, Kha Tran, Mirco Kolarczik, Sophia Helmrich, Alexander W Achtstein, Ulrike Woggon, Nina Owschimikow, Frank Jahnke, et al. Biexciton fine structure in monolayer transition metal dichalcogenides. Nature Physics, 14(12):1199–1204, 2018.

[28] Daniel W Kidd, David K Zhang, and Kálmán Varga. Binding energies and structures of two-dimensional excitonic complexes in transition metal dichalcogenides. Physical Review B, 93(12):125423, 2016.

[29] Ilkka Kylänpää and Hannu-Pekka Komsa. Binding energies of exciton complexes in transition metal dichalcogenide monolayers and effect of dielectric environment. Physical Review B, 92(20):205418, 2015.

[30] Shao-Yu Chen, Thomas Goldstein, Takashi Taniguchi, Kenji Watanabe, and Jun Yan. Coulomb-bound four-and five-particle intervalley states in an atomically-thin semiconductor. Nature communications, 9(1):1–8, 2018.

[31] JP Echeverry, B Urbaszek, Thierry Amand, Xavier Marie, and IC Gerber. Splitting between bright and dark excitons in transition metal dichalcogenide monolayers. Physical Review B, 93(12):121107, 2016.

[32] Cédric Robert, Thierry Amand, Fabian Cadiz, Delphine Lagarde, Emmanuel Courtade, Marco Manca, Takashi Taniguchi, Kenji Watanabe, Bernhard Urbaszek, and Xavier Marie.

Fine structure and lifetime of dark excitons in transition metal dichalcogenide monolayers. Physical Review B, 96(15):155423, 2017.

[33] Yanhao Tang, Kin Fai Mak, and Jie Shan. Long valley lifetime of dark excitons in single-layer WSe_2. Nature communications, 10, 2019.

[34] Sarthak Das, Medha Dandu, Garima Gupta, Krishna Murali, Nithin Abraham, Sangeeth Kallatt, Kenji Watanabe, Takashi Taniguchi, and Kausik Majumdar. Highly tunable layered exciton in bilayer WS_2: Linear quantum confined stark effect versus electrostatic doping. ACS Photonics, 7(12):3386–3393, 2020.

[35] M Zinkiewicz, T Woźniak, T Kazimierczuk, P Kapuściński, K Oreszczuk, M Grzeszczyk, M Bartos, K Nogajewski, K Watanabe, T Taniguchi, C Faugeras, P Kossacki, M Potemski, A Babiński, and M Molas. Excitonic complexes in n-doped WS_2 monolayer. Nano Letters, 21(6):2519–2525, 2021.

[36] Garima Gupta and Kausik Majumdar. Fundamental exciton linewidth broadening in monolayer transition metal dichalcogenides. Physical Review B, 99(8):085412, 2019.

[37] Hongyi Yu, Gui-Bin Liu, Pu Gong, Xiaodong Xu, and Wang Yao. Dirac cones and dirac saddle points of bright excitons in monolayer transition metal dichalcogenides. Nature communications, 5(1):1–7, 2014.

[38] Itai Epstein, Bernat Terrés, André J Chaves, Varun-Varma Pusapati, Daniel A Rhodes, Bettina Frank, Valentin Zimmermann, Ying Qin, Kenji Watanabe, Takashi Taniguchi, et al. Near-unity light absorption in a monolayer WS_2 van der waals heterostructure cavity. Nano Letters, 20(5):3545–3552, 2020.

[39] Medha Dandu, Kenji Watanabe, Takashi Taniguchi, Ajay K Sood, and Kausik Majumdar. Spectrally tunable, large raman enhancement from nonradiative energy transfer in the van der waals heterostructure. ACS Photonics, 7(2):519–527, 2020.

[40] Zhuo Chen, Chonglong Yu, Kai Shum, Jian J Wang, William Pfenninger, Nemanja Vockic, John Midgley, and John T Kenney. Photoluminescence study of polycrystalline $CsSnI_3$ thin

films: Determination of exciton binding energy. Journal of Luminescence, 132(2):345–349, 2012.

[41] Tom J Savenije, Carlito S Ponseca Jr, Lucas Kunneman, Mohamed Abdellah, Kaibo Zheng, Yuxi Tian, Qiushi Zhu, Sophie E Canton, Ivan G Scheblykin, Tonu Pullerits, et al. Thermally activated exciton dissociation and recombination control the carrier dynamics in organometal halide perovskite. The journal of physical chemistry letters, 5(13):2189–2194, 2014.

[42] Rup K Chowdhury, Snehasish Nandy, Sayantan Bhattacharya, Manobina Karmakar, Shivakiran NB Bhaktha, Prasanta K Datta, Arghya Taraphder, and Samit K Ray. Ultrafast time-resolved investigations of excitons and biexcitons at room temperature in layered WS_2. 2D Materials, 6(1):015011, 2018.

[43] Wolfgang Becker. Advanced time-correlated single photon counting techniques, volume 81. Springer Science & Business Media, 2005.

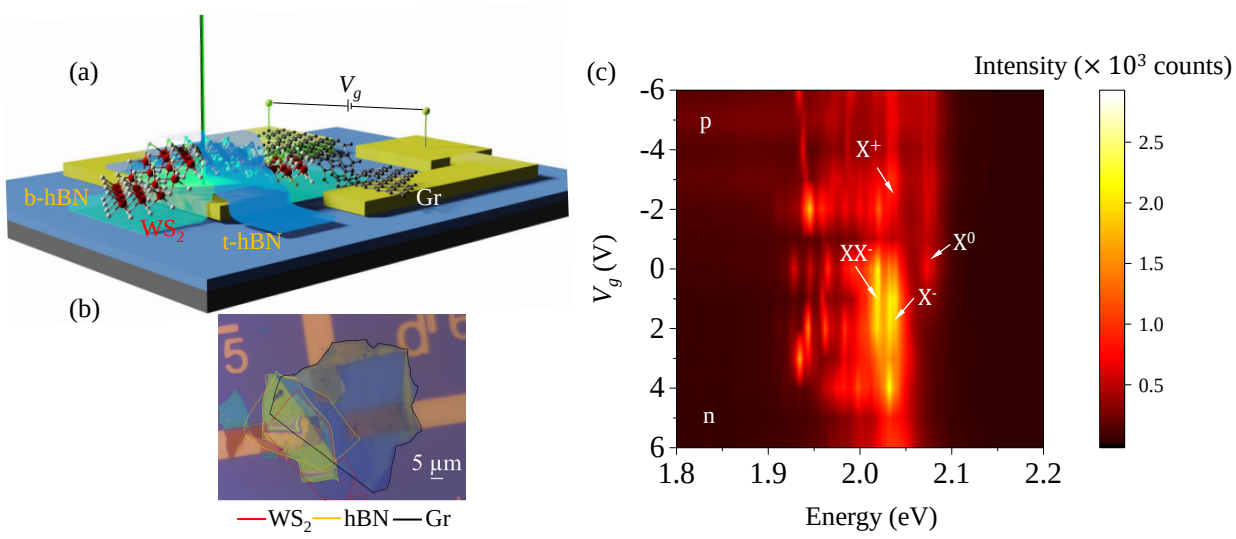


Figure 1: **Device schematic and gate modulation of emission from excitonic complexes.** (a) Schematic and (b) Optical image of the device D1 (1L-WS_2 sandwiched between top and bottom hBN layers) fabricated for controlled electrical doping, a gate voltage (V_g) is applied to the bottom Au electrode while WS_2 is connected to another grounded electrode. (c) Doping dependent intensity variation of exciton (X^0), trion ($X^{\pm}$) and charged biexciton (XX^-) shown and marked (by arrows) in a color plot. The presence of charged biexciton (XX^-) is clearly associated with the presence of both the trion and exciton together.

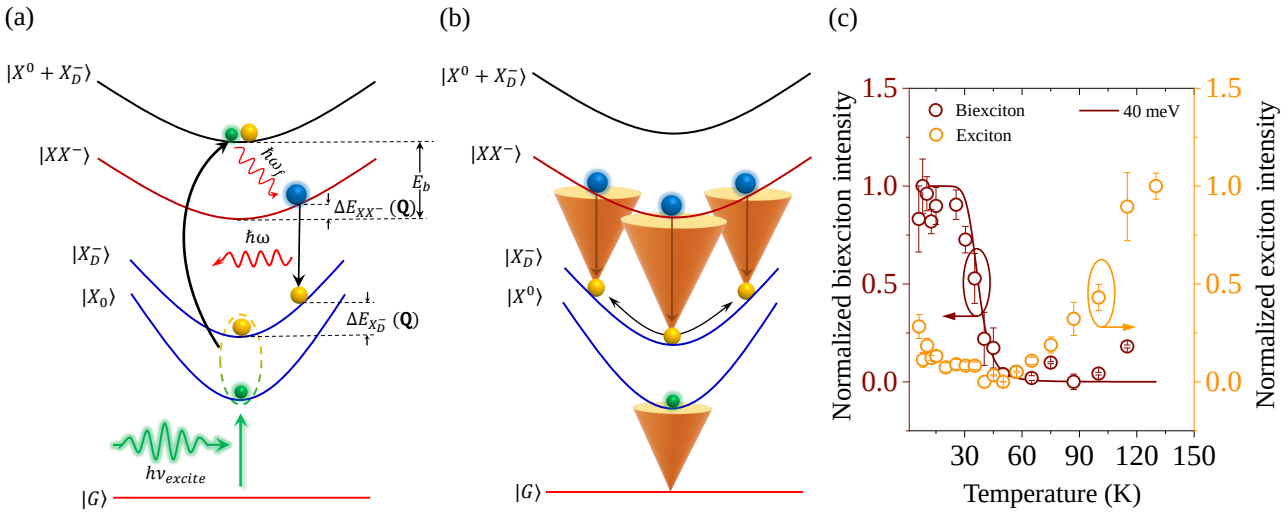


Figure 2: **Model for formation, radiative recombination of charged biexciton and temperature dependent intensity of charged biexciton 1L-WS_2** (a) Creation and recombination of charged biexciton (XX^-) is shown using parallel band model. Dark trion (X_D^-) and bright exciton (X^0) together form XX^-, with a binding energy E_b and a kinetic energy $\Delta E_{XX^-}(Q)$ through the emission of a phonon of energy $\hbar\omega_f$. During recombination, one photon is emitted of energy $\hbar\omega$, and the final state is a dark trion (X_D^-) with a recoil energy of $\Delta E_{X_D^-}(Q)$. (b) Multi-light-cone model for radiative recombination of the charged biexciton. (c) Normalized X^0 and XX^- emission intensities plotted as a function of temperature, indicating opposite trends for X^0 and XX^-. The Fitted traces to the XX^- peak intensity indicate a binding energy of 40 ± 5 meV.

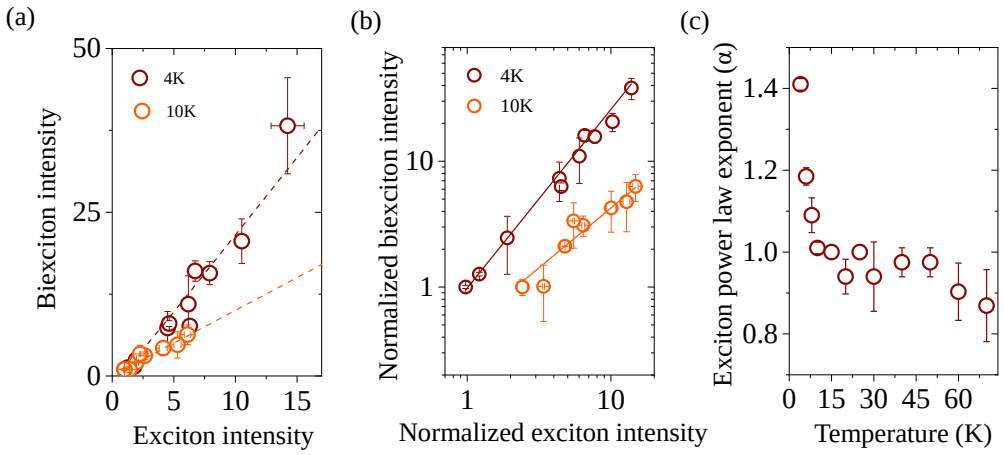


Figure 3: **Temperature dependent kinetics for charged biexciton.** (a) Experimentally obtained intensity of XX^- plotted as a function of the intensity X^0 species (symbols) at 4 K and 10 K. The dashed lines represent the fitted curves obtained from equation 9, plotted at different temperatures. (b) Log-log plot of XX^- intensity with varying exciton (X^0) intensity. The solid lines indicate fits to the approximate power law: ($I_{XX^-} \propto I_{X^0}^{\alpha}$). (c) Plot of the α as a function of temperature, indicating a sharp fall with increasing temperature.

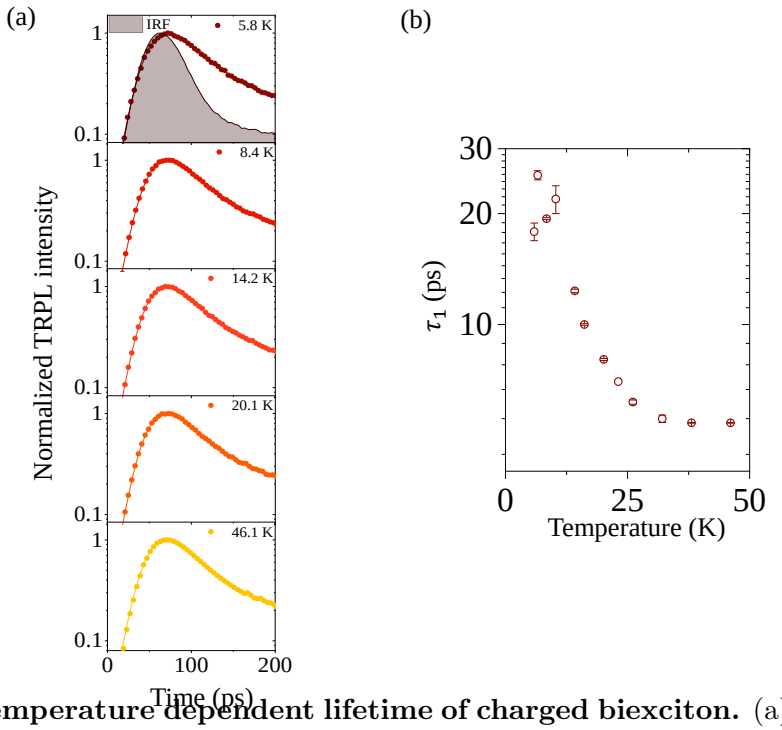


Figure 4: **Temperature dependent lifetime of charged biexciton.** (a) TRPL with varying temperature from 5.8 K to 46.1 K. The symbols represent the measured data, and the solid traces represent the fitted curves (see **Methods**). (b) The decay time plotted as a function of temperature, as obtained from (a).

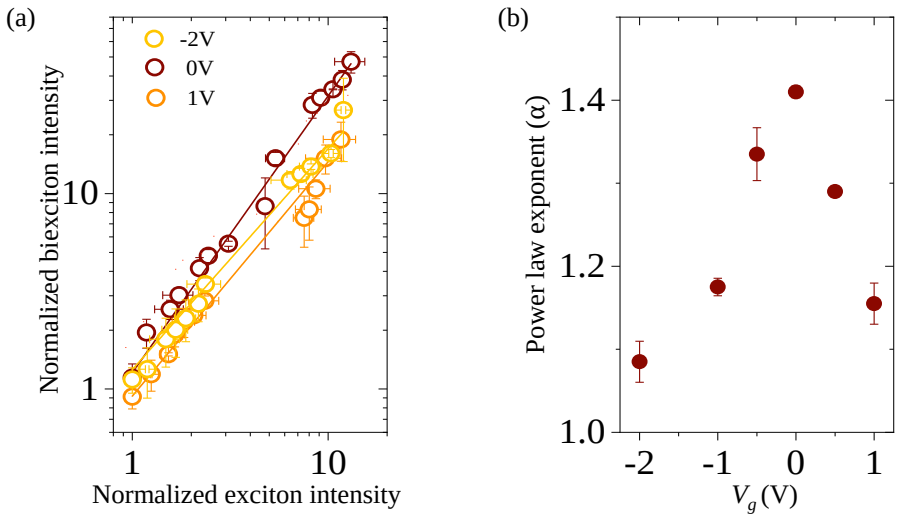


Figure 5: **Gate voltage dependent charged biexciton kinetics.** . (a) Plot of XX^- peak intensity with varying exciton intensity (I_{X_0}) at different V_g. The solid lines indicate X_0 power law fitting: $I_{XX^-} \propto I_{X_0}^{\alpha}$. (b) α plotted as a function of V_g, indicating a sharp decrease of α with $|V_g|$.

Supporting Information:

1. Derivation of temperature dependent dissociation function.

With increasing temperature the total decay rate (R), for charged biexciton (XX^-), can be written as

$$R = \tau_{XX^-}^{-1} + k_0 e^{\frac{-Eb}{k_B T}} \tag{1}$$

Where E_b and τ_{XX^-} are the binding energy and radiative lifetime of XX^- respectively. The Quantum efficiency ($\eta(T)$) for radiative decay is:

$$\eta(T) = \frac{\tau_{XX^-}^{-1}}{R} \tag{2}$$

Equation 2 can be simplified to:

$$\eta(T) = \frac{1}{1 + \kappa e^{-E_b/k_B T}} \tag{3}$$

where $\kappa = k_0 \tau_{XX^-}$ and k_0 is a fitting parameter [1, 2]. Since by measuring PL signal we can only probe radiative decay, equation 3 can be fitted with temerature dependent PL intensity variation of XX^-, shown in the main text Figure 3b.

2. Derivation of steady state coupled exciton (n_{X^0}) and charged biexciton (n_{XX^-}) population equation.

The rate equations are [3, 4]:

$$dn_{X^0}/dt = -n_{X^0}/\tau_{X^0} + \beta_1 P + \gamma_2 n_f n_{XX^-} e^{\frac{-\Delta E_{XX^-}}{k_B T}} - \beta_2 n_{X^0} - \gamma_1 (n_f + 1) n_{X^0} n_{X_D^-} \tag{4}$$

$$dn_{X_D^-}/dt = -n_{X_D^-}/\tau_{X_D^-} + \beta_2 n_{X^0} + \gamma_2 n_f n_{XX^-} e^{\frac{-\Delta E_{XX^-}}{k_B T}} + n_{XX^-}/\tau_{XX^-} - \gamma_1 (n_f + 1) n_{X^0} n_{X_D^-} \tag{5}$$

$$dn_{XX^-}/dt = -n_{XX^-}/\tau_{XX^-} + \gamma_1 (n_f + 1) n_{X^0} n_{X_D^-} - \gamma_2 n_f n_{XX^-} e^{\frac{-\Delta E_{XX^-}}{k_B T}} \tag{6}$$

at steady sate the differentials with respect to time are zero. We can substitute n_{XX^-}/τ_{XX^-}

from equation 6 to equation 5. Then we get a linear relationship between bright exciton and dark trion.

$$n_{X_D^-} = \tau_{X_D^-}\beta_2 n_{X^0} = A_1 n_{X^0} \tag{7}$$

Now, $n_{X_D^-}$ can be replaced by a function of n_{X^0} in the equation 6 and assuming $n_f \approx n_{XX^-}$:

$$n_{XX^-}/\tau_{XX^-} + \gamma_2 n_{XX^-}^2 e^{-\Delta E/k_B T} = \gamma_1(n_f+1)A_1 n_{X^0}^2 \tag{8}$$

From equation 4 we can substitute the n_{X^0} as a function of n_{XX^-} and relation between n_{XX^-} and laser power (P) can be established.

$$\beta_1^2 P^2 C_1 = n_{XX^-}^2[\gamma_2\alpha e^{-\Delta E_{XX^-}/k_B T}(B_1)^2 + C_1/\tau_{XX^-}^2] + 2n_{XX^-}^{3/2}C_1^{1/2}B_1[1/\tau_{XX^-} + \gamma_2 n_{XX^-}\alpha e^{-\Delta E_{XX^-}/k_B T}]^{1/2} + n_{XX^-}/\tau_{XX^-}(B_1)^2 \tag{9}$$

where $B_1 = (\beta_1 + 1/\tau_x)$ and $C_1 = A_1\gamma_1(n_f+1)$

Supporting Figures:

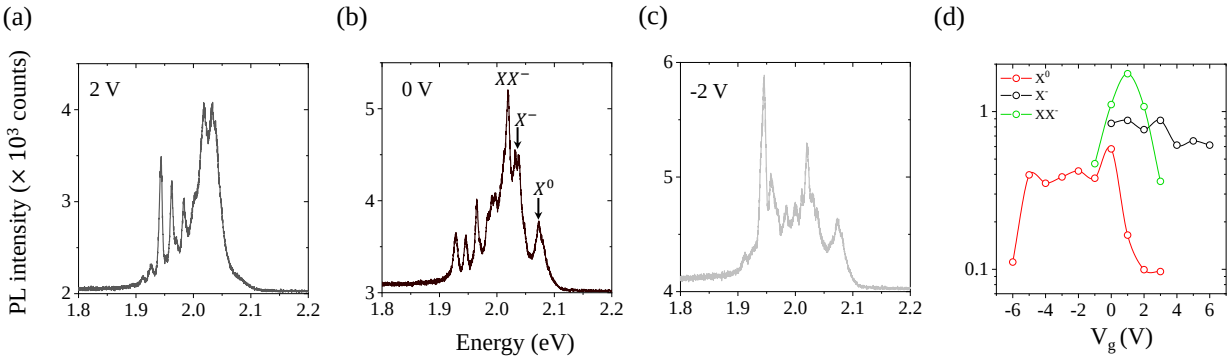


Figure 1: **Gate voltage (V_g) dependent PL spectra obtained at 4 K using cw 532nm laser.** The corresponding gate voltages are shown in left side of the spectra, (b) at $V_g = 0$ V signature of XX^- and other PL peaks such as: exciton (X^0), trion (X^-) are clearly visible. However due to nonpresence of exciton and trion in (a) electron (positive V_g) and (c) neutral (negative V_g) doping region respectively, formation of XX^- is hindered. (d) Fitted PL peak intensities of all the species noted in main text are plotted with V_g (in log scale). Clearly, after $V_g > 3$ V both X^0, and XX^- are not visible.

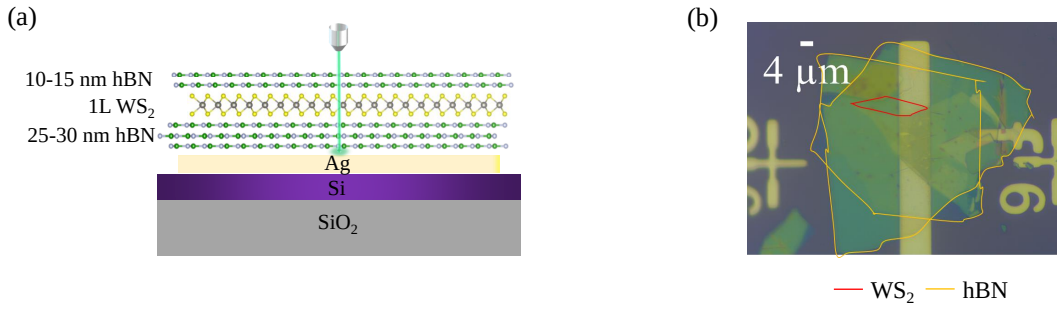


Figure 2: **Schematic and optical image of device D2** (a) Schematic (b) Optical image of Device D2 where top, bottom hBN and 1L WS_2 layers are marked with colored borders. Here 1L WS_2 is kept floating without any applied gate potential (V_g).

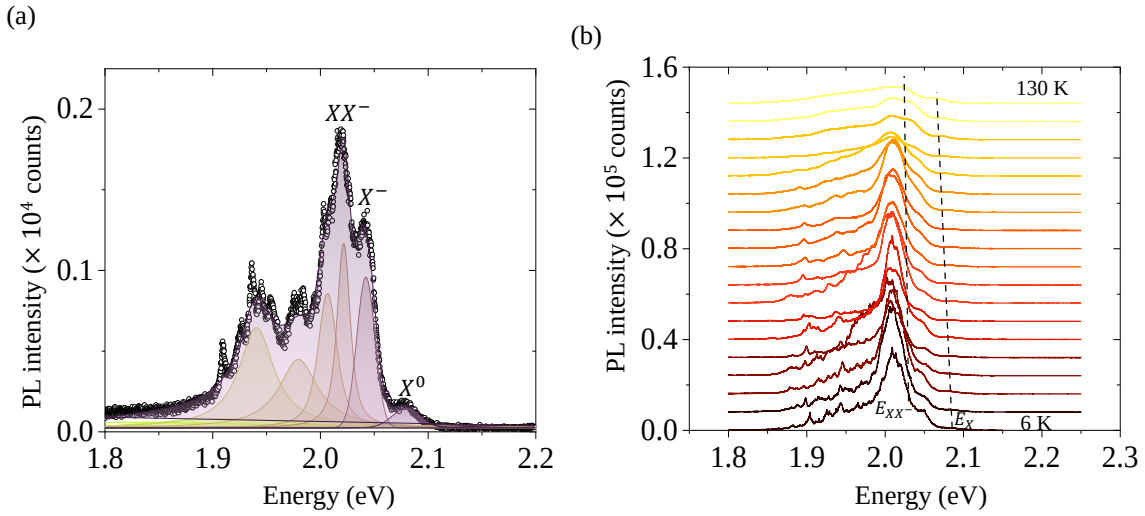


Figure 3: **Fitting of PL spectrum to obtain charged-biexciton (E_{XX^-}) peak position and intensity and spectra at varying temperature.** (a) We fit the obtained spectra with 532 nm cw laser excitation to obtain the XX^- peak position ($\approx$ 2.02 eV) and intensity. (b) Temperature dependent spectra showing XX^- and X^0, intensity values of XX^- peak obtained from this spectra is shown in the main text, Figure 2c.

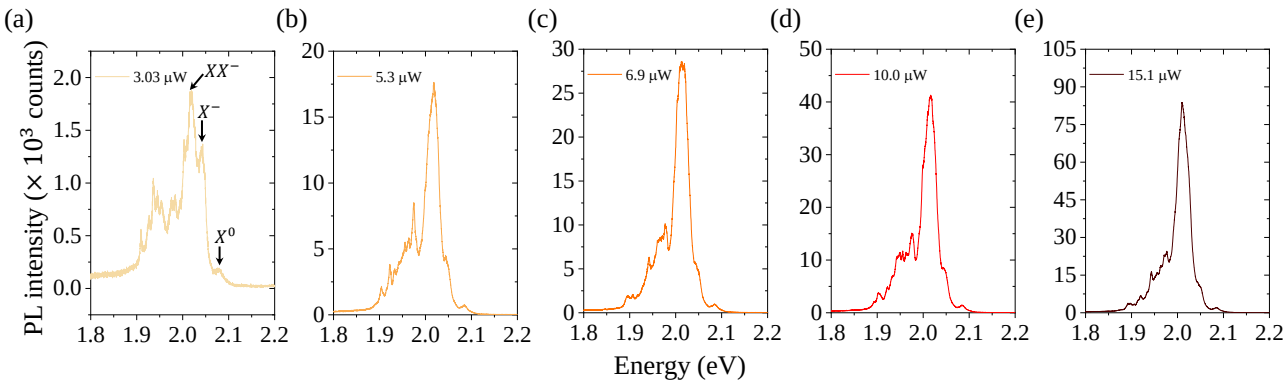


Figure 4: **PL spectra at 4K with varying laser power.** We vary the cw 532 nm laser power from 3.03 μW to 15.1 μW (from (a) to (e)) at 4K to obtain XX^- intensity variation log-log plot shown in the main text Figure 3b and c.

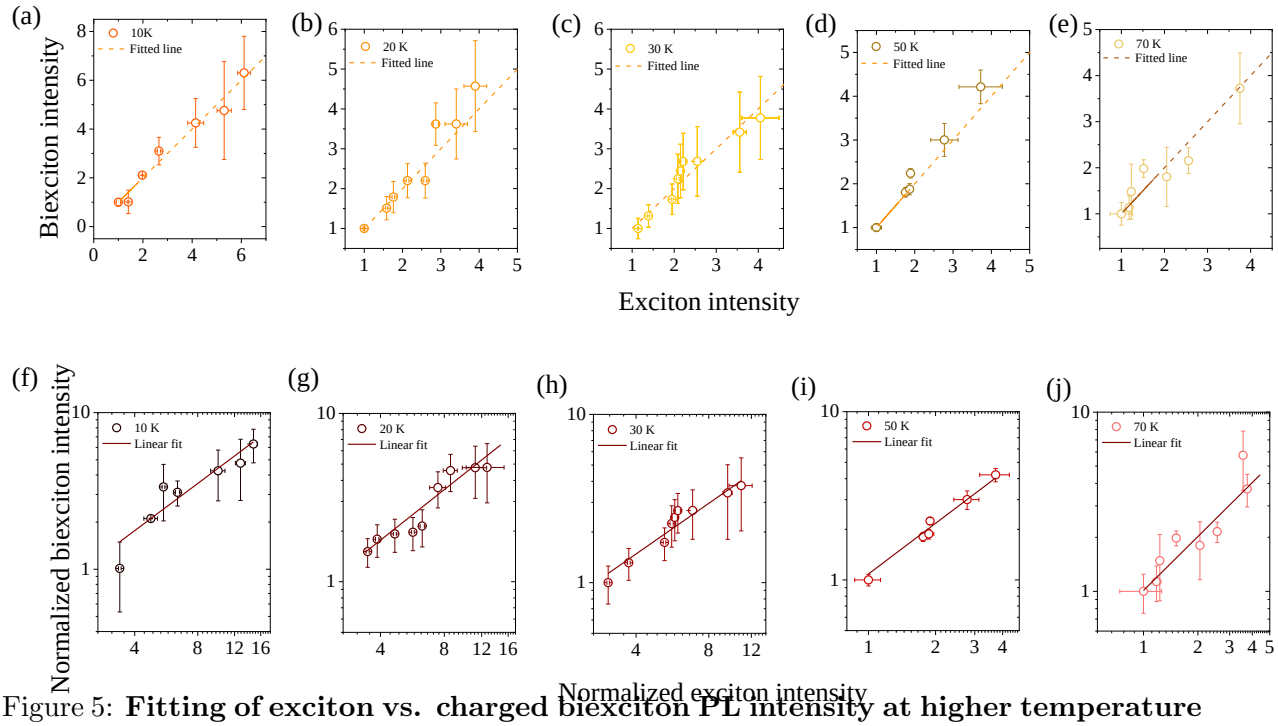


Figure 5: **Fitting of exciton vs. charged biexciton PL intensity at higher temperature points.** Fitting with equation 9 of main text, using dashed line, (top panel, (a)-(e)) and $I_{XX^-} \propto I_{X^0}^{\alpha}$ (bottom panel, f-j), using solid line, for higher temperature range (T = 10, 20, 30, 50 and 70 K) is shown here. After $\approx$ 10K near unity exciton power law is observed.

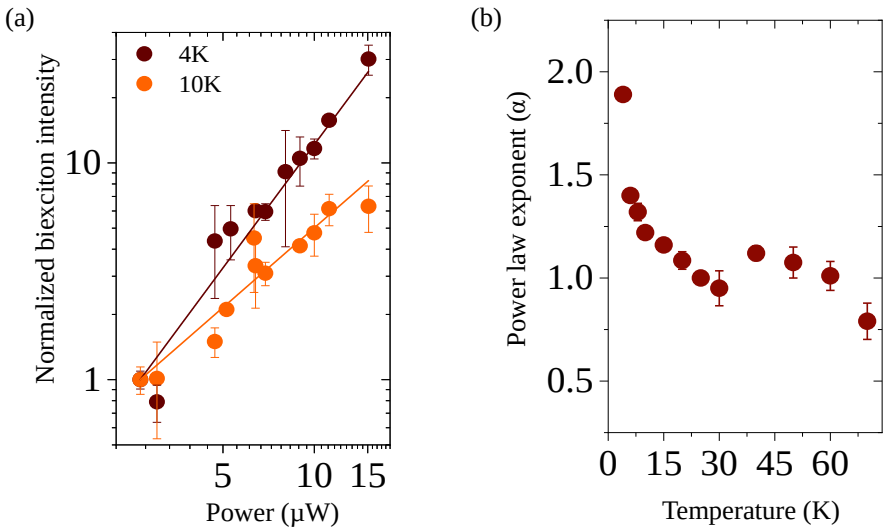


Figure 6: **Charged biexciton intensity with varying laser power at different temperature.** (a) Experimentally obtained XX^- intensity (colored symbols) at 4 and 10K are fitted with $I_{XX^-} \propto P^{\alpha}$ (solid lines). (b) Fitted power law exponent (α) is plotted with varying temperature, showing a downward trend towards near unity power law after $\approx$ 20K.

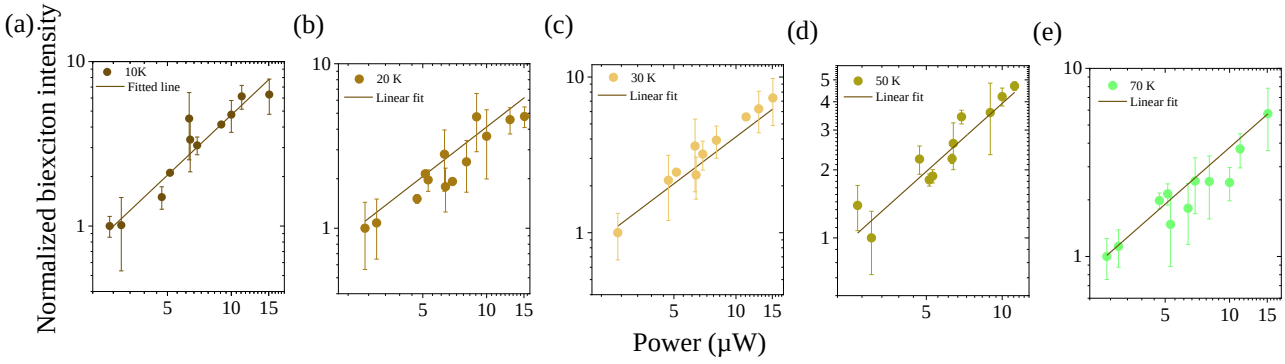


Figure 7: **Laser power law fitting at high temperature points.** Experimentally obtained XX^- PL intensity with laser power at 10, 20, 30, 50 and 70 K ((a)-(e)) are fitted with $I_{XX^-} \propto P^{\alpha}$ (solid lines). After $\approx$ 20K near unity power law is observed.

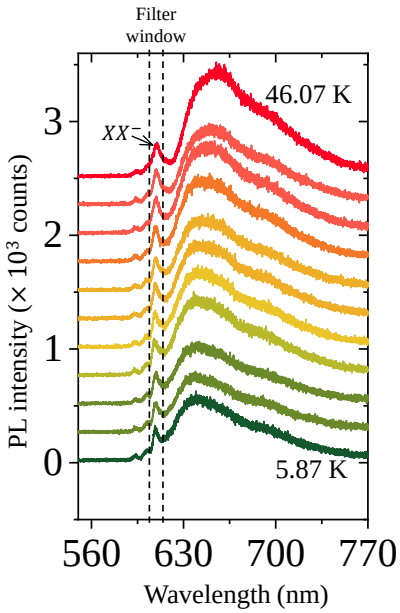


Figure 8: **Temperature dependent in situ PL spectra taken along with TRPL data.** Plot of in situ PL spectra, measured at same temperature points as shown in main text, Figure 4b. The filter window, shown by dashed line, contains XX^- PL emission mostly (marked by arrow).

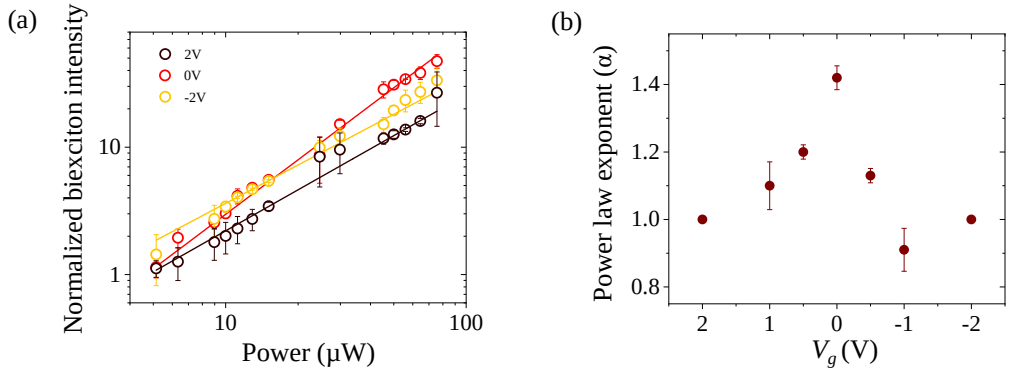


Figure 9: **Gate voltage (V_g) dependent kinetics for charged biexciton.** (a) Plot of XX^- peak intensity with varying laser power (P) at different V_g. The solid traces indicate power law fitting: $I_{XX^-} \propto P^{\alpha}$. (b) α plotted as a function of V_g, indicating a sharp decrease of it with $|V_g|$.

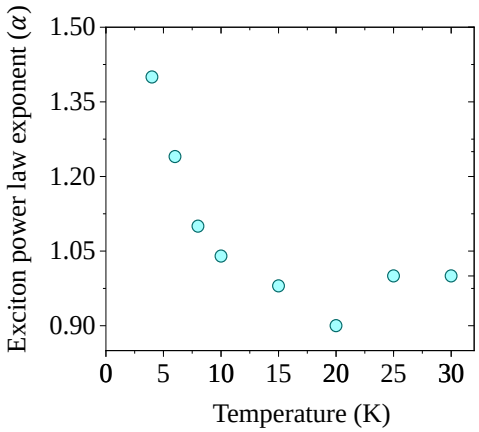


Figure 10: **Exciton power law measurement in sample D1.** With varying Laser power obtained XX^- peak intensity is fitted using $I_{XX^-} \propto I_{X^0}^{\alpha}$ lines and extracted α values are plotted here. This plot is in excellent agreement with main text, Figure 3c.

References

[1] Yumeng You, Xiao-Xiao Zhang, Timothy C Berkelbach, Mark S Hybertsen, David R Reichman, and Tony F Heinz. Observation of biexcitons in monolayer WSe_2. Nature Physics, 11(6):477–481, 2015.

[2] Shao-Yu Chen, Thomas Goldstein, Takashi Taniguchi, Kenji Watanabe, and Jun Yan. Coulomb-bound four-and five-particle intervalley states in an atomically-thin semiconductor. Nature communications, 9(1):1–8, 2018.

[3] VM Asnin, BV Zusov, TM Murina, AM Prokhorov, AA RooAcHEv, and NI Sablina. Radiative recombination of biexcitons in germanium. SOVIET PHYSICS JETP, 35(2), 1972.

[4] Ziliang Ye, Lutz Waldecker, Eric Yue Ma, Daniel Rhodes, Abhinandan Antony, Bumho Kim, Xiao-Xiao Zhang, Minda Deng, Yuxuan Jiang, Zhengguang Lu, et al. Efficient generation of neutral and charged biexcitons in encapsulated WSe_2 monolayers. Nature communications, 9(1):1–6, 2018.